On the Far Field Optical Properties of Ag−Au Nanosphere Pairs

Ezequiel R. Encina and Eduardo A. Coronado*

INFIQC, CLCM, Departamento de Fisicoquímica, Facultad de Ciencias Químicas, Universidad Nacional de Córdoba, Córdoba, 5000 Argentina

Received: June 15, 2010; Revised Manuscript Received: August 27, 2010

In this work we study the far field optical properties of heterodimers composed of a silver and a gold nanosphere of the same size, by means of exact electrodynamics calculations based on the generalized multiparticle Mie theory. We analyze the effect of the incident polarization, nanosphere separation, radius and dielectric media on the optical response. The on resonance angular distribution of the scattered radiation is also analyzed. The nonsymmetrical features of this system allow us to evaluate and perform a careful examination of the contributions of absorption and scattering from each individual nanosphere to the total extinction of the system. At variance with the homodimer system, the heterodimer exhibits a simultaneous shift of two plasmonic resonances. This feature constitutes a very useful and accurate way to calibrate both interparticle distance and size at the same time for a given dielectric environment. In this way, we provide a general and complete description of the far field optical properties of this particular nanostructure, which may be valuable for the design and development of plasmonic devices and optical tools and could serve as benchmark calculations for future comparisons with experiments.

Introduction

Noble metal nanoparticles (NPs) are well-known because they are able to sustain localized surface plasmon resonances (LSPR), which are collective oscillations of the conduction electrons in response to an incident electromagnetic field.[1,2] The LSPR frequency can be tuned in the UV-NIR spectral range by changing the NP size, shape and surrounding media.[3] As a result of plasmon oscillation, substantial enhancements of the extinction cross section and of the electric field around the NP are observed.[4] These phenomena give rise to the application of NPs in several fields such as chemical and biological sensing,[5−7] photocatalysis,[8,9] and solar energy conversion.[10−12]

In NP aggregates, the interparticle separation is a relevant parameter that strongly modifies the optical response of nanostructured materials. This issue has been extensively studied both experimental and theoretically by several authors, particularly for NPs pairs of the same metal (homodimers).[13−31] In this kind of nanostructures, the longitudinal dipole LSPR shows a significant redshift as the interparticle separation decreases for incident polarization parallel to the homodimer axis. This change in the optical response of the system as a consequence of plasmon coupling, is more pronounced for Ag than for Au nanospheres pair.[32] This behavior can be used as a plasmon ruler if a proper calibration of the resonance wavelength shift ($\Delta\lambda_{res}$) with NP separation is achieved. In this respect, we have recently found an accurate resonance condition for Ag nanosphere pairs.[33] These plasmonics devices have the advantage of being able to measure distances in a wider range (5−100 nm) compared with other techniques, such as FRET (1−10 nm).[17] Furthermore, larger enhancements of the electric field between the particles are observed in comparison with isolated NPs, which have important implications in surface enhanced spectroscopies.[19]

However, to the best of our knowledge, there are only a few studies concerning the optical properties of NPs pairs given by a Ag and a Au particle (heterodimer). In this respect, Pinchuk et al. have modeled the optical properties of Ag and Au NPs aggregated by electrostatic interactions into closely packed clusters, and concluded that the optical response of mixtures of oppositely charged aggregating NPs can not be accurately described by linear combination of the components' individual spectra and require higher-level theoretical treatment.[34] More recently, Bachelier et al. have theoretically investigated the near-field coupling between a Au and Ag nanospheres.[35] They found the presence of Fano profiles in the absorption cross section of the Au NP due to the coupling between the spectrally LSPR of the Ag NP and the continuum of interband transitions of the Au NP. These Fano resonances are strongly enhanced while decreasing the gap between the nanospheres until the Au NP is fully included in the near field region of the Ag NP. In spite of all of these efforts, a systematic study of the optical properties of these heteronanostructures has not been comprehensively addressed yet. In particular, the effects of symmetry breaking on the optical properties in the transition from homo to heterodimers are not completely understood and deserve to be studied more deeply as it may give rise to interactions of different nature with the possible observation of new optical phenomena, which could be important from both scientific and technological standpoints.

The goal of this work is to study, by means of exact electrodynamics calculations, the far field optical properties of heterodimers composed of Ag and Au nanospheres of the same size. The effects of incident polarization, nanospheres diameter *D*, center to center separation *S*, and dielectric environment on the extinction cross section are analyzed, and also the absorption and scattering contributions from each individual nanosphere to the total extinction of the system are examined. The angular distribution of the light scattered by the heterodimers at some representative resonance frequencies, important for future applications in plasmon spectroscopy, is also characterized. In addition, the optical response of these heterodimers is compared with that of homodimers, and its possible application in plasmonic rulers is discussed.

* Corresponding author. E-mail: coronado@fcq.unc.edu.ar.

10.1021/jp105522b
Published on Web 09/15/2010

Methodology

The optical response of Ag−Au nanospheres heterodimers was computed using the Generalized Multiparticle Mie Theory (GMM) formulation developed by Xu. This valuable method is a suitable and rigorous formulation of the scattering problem able to exactly solve the complex problem of interaction between an electromagnetic field and an aggregate of spheres. The GMM method has been described in detail in several places, so we will only give a brief summary here.[36,37] In the GMM method, scattered fields from each L individual sphere are solved in terms of the respective sphere-centered reference systems. In an arbitrarily chosen primary jth coordinate system, the Cartesian coordinates of the origins of these L displaced coordinate systems (i.e., the sphere centers) are (X^j, Y^j, Z^j), $j = 1, 2, ..., L$. In order to solve multisphere-scattering through the Mie-type multipole superposition approach, the incident plane wave is expanded in terms of vector spherical wave functions in each of the L sphere-centered coordinate system. Thus, the total electromagnetic field incident upon each sphere in the aggregate is obtained, which consist of two parts: (1) the initial incident plane wave and (2) the scattered waves from all other spheres in the aggregate. The next step, of vital importance to achieve a complete multisphere light-scattering solution, is to construct a single field representation for the total scattering field from the aggregate as a whole by expanding it in vector spherical wave functions. Finally, with the total scattered field at hand, and based on the analytical expressions for amplitude scattering matrix of an aggregate of spheres, it is possible to derive a rigorous formula for other fundamental scattering properties such as extinction, absorption, and scattering cross sections.[36,37] An important feature of the GMM formulation is that it allows us to analyze the individual contributions coming from each sphere of the NP pair, particularly relevant for heterostructures. For instance, the extinction efficiency for a Ag−Au nanosphere pair can be written as:

$$Q_{\text{ext,pair}} = Q_{\text{ext,Ag}} + Q_{\text{ext,Au}}$$

Analogous expressions can be also written for the absorption and scattering extinction efficiencies. It should be pointed out that the extinction efficiency has been calculated by dividing the extinction cross section by the sum of the areas of the geometrical cross sections of each sphere. In all the calculations presented in this work, the direction of the incident wave-vector k is perpendicular to the line that connects the spheres centers (from now on, dimer axis), and the dielectric function tabulated by Palik for Ag and Au was employed.[38] For each dimer analyzed, the separation parameter between the nanospheres σ, defined equal to the ratio between S and D (see scheme in Figure 4 for a graphic illustration) is large enough ($\sigma \geq 1.05$) so that nonlocal effects on the dielectric constant can be neglected.[39]

Results and Discussion

1. Influence of the Incident Polarization. Figure 1 shows the extinction spectra of a $D = 30$ nm heterodimer in vacuum for two extreme cases: $\sigma = 3$ and 1.05 under parallel (black curve) and perpendicular (red curve) incident polarization with respect to the dimer axis. These results clearly illustrate, as it has been previously found, that the optical properties of noble metal dimers are highly sensitive to the interparticle separation. For relatively large interparticle separations ($\sigma = 3$, Figure 1A), the optical response of the heterodimer is indistinguishable from the half-sum of the extinction efficiency of the individual

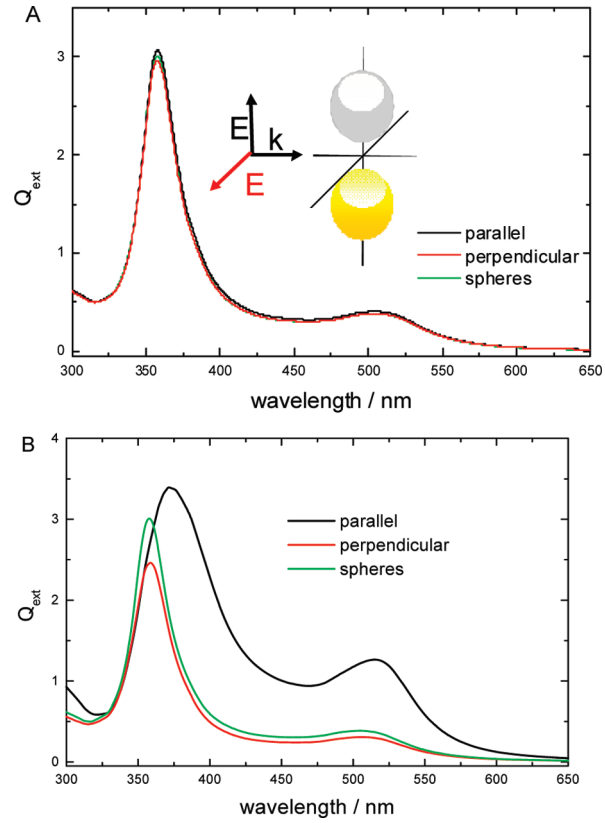

Figure 1. Effect of the incident polarization on the extinction efficiency of a heterodimer in vacuum ($D = 30$ nm) for $\sigma = 3$ (A) and 1.05 (B). The half-sum of the extinction efficiency of the isolated nanospheres is also plot for comparison (green line). The inset in panel A schematically shows the illumination configuration.

nanospheres, whatever the incident polarization, which indicates that at such a distance there is almost no interaction between the nanospheres. The spectra shows two peaks at $\lambda = 360$ and 505 nm, which are associated to the dipole LSPR of the Ag and Au nanosphere, respectively. In the opposite case, i.e. for very small interparticle separations ($\sigma = 1.05$, Figure 1B) remarkable changes in the extinction spectra are observed for incident polarization parallel to the dimer axis: both peaks are red-shifted (the peak associated to the LSPR of the Ag nanosphere is now at $\lambda = 380$ nm, while that associated to the Au NP is at $\lambda = 520$ nm). Another important feature is that both peaks broaden and increase their extinction efficiency. For incident polarization perpendicular to the dimer axis, the optical response is quite similar to that of the half-sum of the isolated nanospheres, indicating that for this configuration there is not significant interaction between the particles, in spite of the fact that they are relatively close to each other. Thus, hereafter we will focus our attention on the configuration corresponding to incident polarization parallel to the dimer axis. To address the origin of such spectral changes, we will now analyze the individual contributions of absorption and scattering to the total extinction of the system.

2. Influence of the Nanosphere Diameter and Its Partial Contributions to Extinction. Figure 2 shows the variation of the extinction spectra for Ag−Au heterodimers in vacuum ($D = 10$ nm), together with the partial contribution to absorption and scattering from each metal, as the nanospheres are getting closer, i.e., as $\sigma \rightarrow 1$. Specifically we show the spectra for some representative values of $\sigma = 1.5$, 1.3, and 1.05 in panels A−C, respectively. For this small size, the scattering is negligible whatever the interparticle separation, and the extinction is

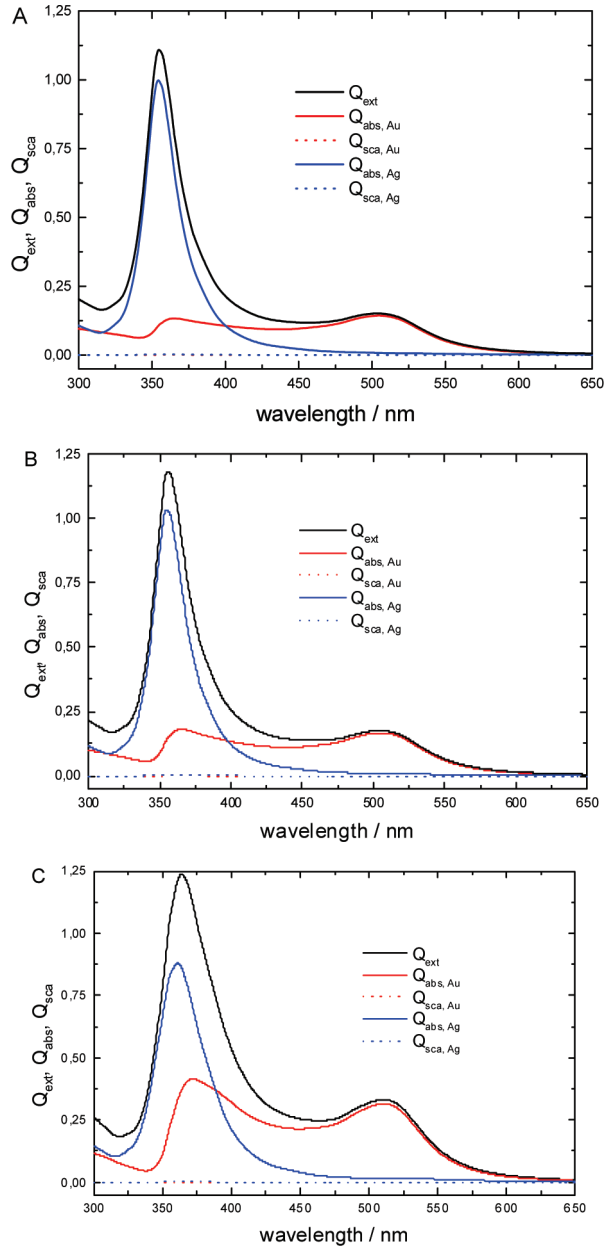

Figure 2. Variation of the extinction spectra for Ag−Au heterodimers in vacuum ($D = 10$ nm), for incident polarization parallel to the dimer axis, as the interparticle separation is decreased, together with the contributions due to absorption and scattering from each nanosphere. $\sigma = 1.5$ (A), 1.3 (B), and 1.05 (C).

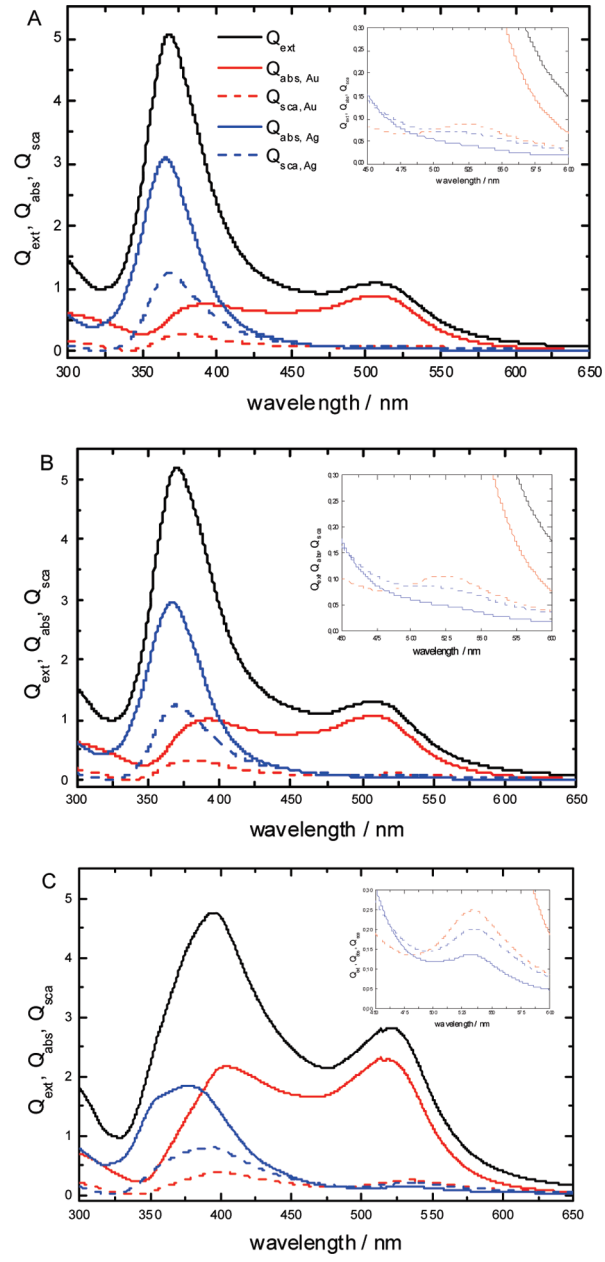

Figure 3. Variation of the extinction spectra for Ag−Au heterodimers in vacuum ($D = 50$ nm), for incident polarization parallel to the dimer axis, as the interparticle separation is decreased, together with the contributions due to absorption and scattering from each nanosphere. $\sigma = 1.5$ (A), 1.3 (B), and 1.05 (C). The inset on the top right side of each panel is a zoom view of the spectra in the 450−550 nm wavelength range.

completely due to absorption. Figure 2A ($\sigma = 1.5$) clearly shows that the extinction peaks at $\lambda = 355$ and 504 nm are due to the dipole LPSR of the Ag and Au nanospheres, respectively. However, $Q_{abs,Au}$ also shows an additional peak at $\lambda = 365$ nm, which is identified as a Fano profile, in agreement with the results recently reported by Bachelier et al.[35] This Fano profile is explained by the near field coupling between the interband transitions continuum of the Au nanosphere and the discrete LSPR of the Ag NP. Reducing σ to 1.3 does not produce any qualitative change on the extinction spectrum as the respective peaks are slightly red-shifted and become more intense, in particular the one associated with the Fano profile. If the separation is decreased to $\sigma = 1.05$ important changes in the optical response are observed. The extinction efficiency depicts two peaks at $\lambda = 364$ and 510 nm due to the remarkable red-shift of the absorption peak associated with the partial contribution of the Ag LSPR, which becomes broader and less intense, and to the contribution of the peaks associated to the dipole LSPR and Fano profile of the Au particle, which are now of greater intensity.

For heterodimers of spheres of larger diameter ($D = 50$ nm, Figure 3), the variation of the extinction spectra as $\sigma \rightarrow 1$ follows qualitatively the same trend than the small heterodimer ($D = 10$ nm), i.e. the extinction peaks are red-shifted and broader. However, the magnitude of the shifts is higher in the present case than for $D = 10$ nm, which could be attributed in part to retardation effects. In particular, the extinction peaks shifts from $\lambda = 368$ to 395 nm and from $\lambda = 506$ to 521, as σ decreases from 1.5 to 1.05. The broadening as well as the decrease in intensity of the peak associated with $Q_{abs,Ag}$ as $\sigma \rightarrow 1$ can be

attributed to a red-shifted of the dipole LSPR (378 nm) while higher order LSPR remains almost unchanged (those at λ near 365 nm). This situation is analogous to the variation of the extinction peaks of a single sphere as the diameter is increased: the higher order resonances are less sensitive to changes in the NP size remaining at higher energies in the spectra, while the dipole mode considerably broadens and redshifts. The Fano profile associated to the Au nanosphere also redshifts and increase its intensity as σ decreases from 1.5 to 1.05, being the main contribution to the extinction for $\sigma = 1.05$ (Figure 3C). Comparing both heterodimers, the most important qualitative difference is that for $D = 50$ nm Q_{sca} has appreciable contributions from both metals, particularly between 360 and 410 nm. The enhancement of $Q_{sca,Ag}$ in this spectral range is due to the scattered radiation after the excitation of the dipole LSPR. The nature of the process that produces the enhancement of $Q_{sca,Au}$ can be attributed to a scattering induced by near field coupling. In turn, the increments of $Q_{sca,Au}$ and $Q_{sca,Ag}$ around $\lambda = 530$ nm, which are low but significant, could be associated to the scattered radiation by the dipole LSPR excited in the Au nanosphere and to the near field coupling induced radiation scattered by the Ag one, respectively. We have checked the assumption that the scattered radiation by the off resonance sphere is intimately related to a near field mechanism. This effect can be explained by noting that the enhancements of $Q_{sca,Au}$ and $Q_{sca,Ag}$ at $\lambda = 400$ and 530 nm, respectively are absent in the corresponding spectra of the isolated nanospheres. A basic principle of optics states that previous to any scattering process it is necessary an excitation one. Therefore, it is reasonable to inquire about the nature of the excitation process in the off resonance nanosphere. We propose that, in a similar fashion to the near field coupling that originates the Fano profile, the on resonance particle transfer the plasmon energy to the off resonance one through a near field coupling of the respective LSPR. This excitation energy is then converted into scattered light. Additionally, the values of $\int_{350}^{450} Q_{sca,Au}\, d\lambda$ and $\int_{500}^{575} Q_{sca,Ag}\, d\lambda$, which can be interpreted as a measure of the mean amount of radiation scattered, increase from 17.1 to 26.6 and from 4.5 to 12.7, respectively, as σ decreases from 1.5 to 1.05. This trend suggests that these enhancements of Q_{sca} are more important at smaller interparticle distances, indicating that a near field mechanism is involved. As far as we know, this kind of plasmonic energy transfer has not been reported, and to give a detailed description of the physical origin of the Au scattering resonance in the blue, as well as the Ag scattering resonance in the red, a further particular and exhaustive study of this phenomenon is necessary. In order to achieve a deeper understanding of this phenomenon we are currently performing near field calculations, which will be the subject of future work.

To finalize this subsection it is worth to mention experimental work on the optical properties of the Ag ($D = 30$ nm)−Au ($D = 40$ nm) heterodimer recently published by Sheikholeslami et al.[40] Although the size of this heterodimer is different from those studied here, we will perform a qualitative comparison. In general, the simulated spectra presented here are in agreement with the experimental spectra, as the latter also displays, for longitudinal polarization, two scattering peaks both red-shifted with respect to the isolated Ag and Au spheres. In addition, these authors state that the plasmon hybridization model[24] fails to account for this behavior because it does not take into account the coupling between the Ag LSPR and the Au interband transitions. It is important to mention that their measurements correspond to the scattering of the heterodimer as a whole, i.e., $Q_{sca} = Q_{sca,Ag} + Q_{sca,Au}$. The present work provides, by means of GMM simulations, further insight on this system by analyzing the individual contribution arising from each sphere.

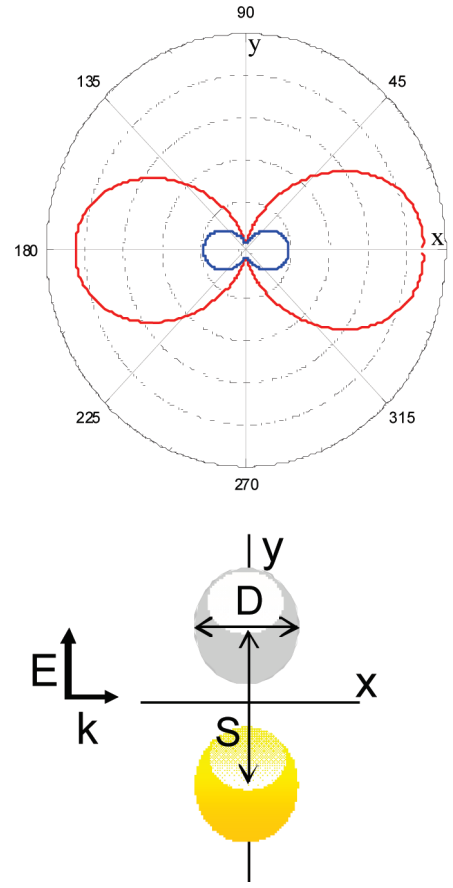

Figure 4. Polar plot of the scattered radiation in the *xy* plane generated by a $D = 50$ nm and $\sigma = 1.05$ heterodimer in vacuum, when the incident polarization is parallel to the dimer axis. The illumination configuration is schematically shown at the bottom. Red curve (blue curve) corresponds to incident wavelength of $\lambda = 395$ nm ($\lambda = 521$ nm).

3. Angular Scattering Properties. To further characterize the far field optical properties of the heterodimers in this section we will examine the angular distribution of the scattered radiation at some representative wavelengths. Figure 4 shows in a polar plot the scattering patterns for $D = 50$ nm and $\sigma = 1.05$ heterodimer in the scattering plane *xy* (see scheme below in Figure 4), for two incident wavelengths, $\lambda = 395$ and 521 nm, where Q_{sca} peaks. Note that the polar patterns correspond to the radiation intensity scattered by the nanostructure as a whole. Whatever the excitation wavelength, both scattering patterns are symmetrical around the *x* axes and depict two lobules of equal intensity in the forward and backward directions, i.e., 0° and 180°, respectively. In addition, at both wavelengths there is no radiation scattered in the direction of the incident electric field. Both patterns resemble the one corresponding to a point emitting dipole, which support our previous assignment of the LSPR multipole order excited at each wavelength. In addition, the amount of scattered light at $\lambda = 395$ nm (red curve) is almost 5 times more intense than at $\lambda = 521$ nm (blue curve), in agreement with the respective values of Q_{sca}. This observation indicates that it could be possible to change between switch off/on scattering regimes but keeping substantial absorption efficiencies by controlling the incident wavelength, an interesting feature for active plasmonic devices. Moreover, it should be also mentioned that, as expected, the amount of light scattered is directly proportional to *D*, as can

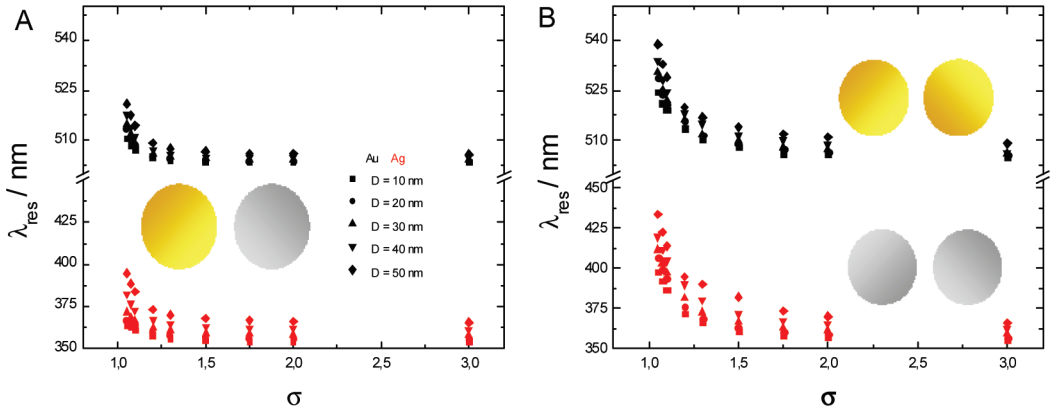

Figure 5. (A) Dependence of the spectral position of the extinction peaks of heterodimers in vacuum, i.e., $\lambda_{res,Ag}$ and $\lambda_{res,Au}$, on σ for the size range studied, when the incident polarization is parallel to the dimer axes. (B) Dependence of the longitudinal dipole LSPR spectral position of Ag and Au homodimers in vacuum on σ for the same size range than in A.

be appreciated from the values of Q_{sca} in Figures 2C and 3C. In fact, the intensity scattered by the $D = 10$ nm heterodimer is completely negligible.

4. Comparison between Homo and Heterodimers and Their Potential Use as Plasmonic Nanorulers. The dependence of the spectral position of the extinction peaks, i.e., $\lambda_{res,Ag}$ and $\lambda_{res,Au}$, on σ is summarized in Figure 5A for the size range studied here. In general, this dependence is nearly exponential for both $\lambda_{res,Ag}$ and $\lambda_{res,Au}$. Moreover, it is also clear that, for a given σ value, the magnitude of the red shift increases with the nanostructure size, and that the spectral position of the extinction peaks does not significantly change for $\sigma \geq 1.5$. Note that the respective λ_{res} values are the result of the different contributions to extinction described in section 2 above. For comparison, in Figure 5B we show the dependence of the longitudinal dipole LSPR spectral position on σ for Ag and Au homodimers in the same size range. At first glance it is observed that for given σ and D values, the magnitude of the shift is higher for the homo than for the heterodimer, which is more pronounced for $\sigma \leq 1.5$. These trends are reasonable because in the homodimer there are two main factors that contribute to the redshift: retardation effects and plasmon coupling. Instead, in the heterodimer, retardation effects are the main contribution to the plasmon shifts, as plasmon coupling is less important due to the mismatch in the respective plasmon energies introduced by the broken symmetry. Besides these quantitative differences, it is worth to remark that the extinction spectra of heterodimers depicts two plasmonic shifts, instead of one as occurs in homodimers, a property that could be used for the design of more accurate plasmonic rulers by making use of the dependence of both λ_{res} on σ, with potential applications in biological systems, for example. In order to work properly these devices require an accurate calibration of the dependence of λ_{res} on σ. As a consequence of the two plasmonic shifts in the heterodimers, it is possible to build simultaneously two calibration curves, i.e., the dependence of $\lambda_{res,Ag}$ and $\lambda_{res,\ Au}$ on σ for each diameter. To illustrate the potential use of these heterodimers as a nanoruler, we give in Figure 6 a hypothetical example where it is shown that the two calibration curves can be used simultaneously to determine both the size and interparticle separation. Suppose that the extinction spectrum of a given heterodimer in vacuum peaks at 518 and 389 nm, respectively (green lines). These λ_{res} values just completely match with the values corresponding to the $D = 50$ nm and $\sigma = 1.075$ heterodimer. Note that the $D = 40$ nm and $\sigma = 1.05$ heterodimer also shows an extinction peak at 518 nm, but the resonance associated with the Ag sphere peaks at 382 nm, which is 7 nm bellow the resonance value of

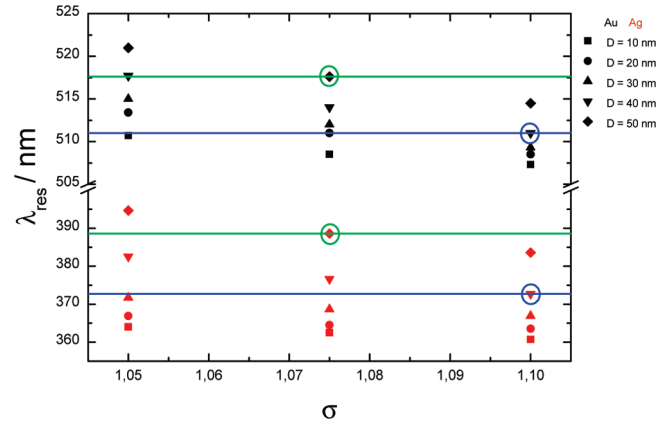

Figure 6. Dependence of the spectral position of the extinction peaks of heterodimers in vacuum, i.e. $\lambda_{res,Ag}$ and $\lambda_{res,Au}$, on σ when the incident polarization is parallel to the dimer axes. This figure exemplifies how it is possible to determine simultaneous and unambiguously both the size and interparticle separation of a given heterodimer by means of the calibration curves and by knowing the values of $\lambda_{res,Ag}$ and $\lambda_{res,Au}$ for two heterodimers. The respective blue and red circles indicate the heterodimers that match the given $\lambda_{res,Ag}$ and $\lambda_{res,Au}$ values.

389 nm. Another example is shown in blue lines which correspond to λ_{res} values of 511 and 373 nm, respectively. Note that in this case there are several heterodimers that display resonance values at 511 nm as well as 373 nm, but there is only one ($D = 40$ nm and $\sigma = 1.1$) that completely match both λ_{res} values. Therefore, by knowing the respective λ_{res} values it is possible to determine unambiguously both the size and interparticle separation of a given heterodimer by means of the two calibration curves. However, it is important to mention that in spite of the improved capabilities of these heterodimers for nanometrological measurements, distances and sizes could be determined in a simultaneous and accurate way for the range $1.05 \leq \sigma \leq 1.3$. This is so because for both plasmonic resonances the variation of λ_{res} on σ, for $\sigma \geq 1.3$, is not very important as shown in Figure 5A. Considering that, depending on the NP size, the extinction spectra could be dominated by Q_{abs}, conventional spectroscopic techniques to perform single particle measurements, such as darkfield or TIR, could not be suitable. In these cases, the use of nonconventional spectroscopic techniques using lock-in detection methods, such as the recently developed spatial-modulation far-field optical technique combined with a frequency tunable light source,[41−43] should be more appropriate for a practical implementation of the proposed plasmonic ruler. The relative magnitudes of the spectral shifts

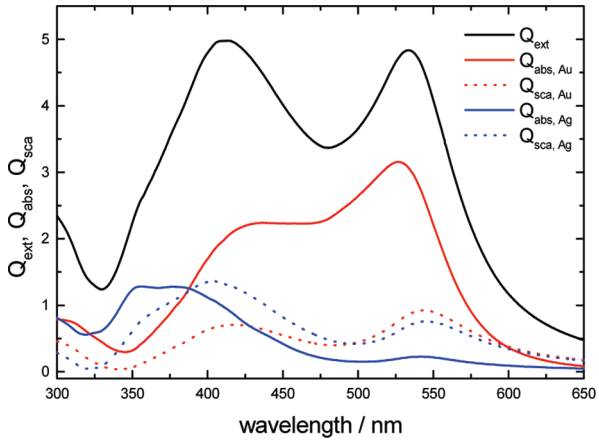

Figure 7. Extinction spectrum of a $D = 50$ nm and $\sigma = 1.05$ heterodimer in water along with its respective partial contributions of absorption and scattering from each individual nanosphere, when the incident polarization is parallel to the dimer axes.

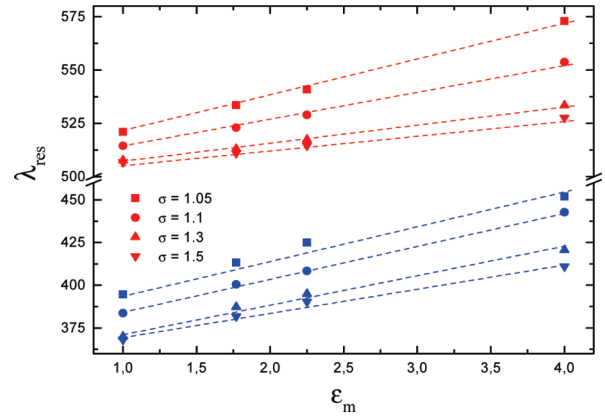

Figure 8. Dependence of $\lambda_{res,Ag}$ and $\lambda_{res,Au}$ on the environment dielectric constant ε_m, for $D = 50$ nm heterodimers at several σ values. Dashed lines are plotted to guide the eye.

seem to be much smaller than for Au−Au or especially Ag−Ag pairs. This seems to be a significant disadvantage for the sensitivity of the proposed rulers. However, the heterodimer exhibit two simultaneous plasmon shifts. Therefore this disadvantage is only apparent because a given set of plasmon shifts would only fit with only one interparticle separation, even if the magnitude of both shifts is relatively smaller compared to the homodimer.

5. Influence of Dielectric Environment on the LSPR Shift. In the analysis performed above, we have been dealing with heterodimers in vacuum, an ideal situation convenient to conceptually study the interactions involved and to describe quantitatively the optical response of real nanostructures in air. However, for the majority of applications in chemistry and biology, the nanostructures are in a dielectric environment different from air. Therefore, in this last section, we will analyze the effects of the dielectric environment on the optical response. In general, the effect of increasing the dielectric constant of the media, ε_m, produces a redshift of both $\lambda_{res,Ag}$ and $\lambda_{res,Au}$. Nonetheless, to gain a deeper insight into the effects of increasing ε_m on the optical response, we show in Figure 7 the extinction spectrum of the $D = 50$ nm and $\sigma = 1.05$ heterodimer in water along with the respective absorption and scattering contributions from each sphere. To better appreciate the changes in the spectra it is worthwhile to make a comparison with the corresponding nanostructure in vacuum (Figure 3C). As mentioned above, the redshifts of $\lambda_{res,Ag}$ and $\lambda_{res,Au}$ are due to the changes in the absorption and scattering efficiency. In the spectral region between 350 and 450 nm, the different contributions peak at different wavelengths and each resonance depicts a much greater spectra broadening. The Fano profile appears in water as shoulder at $\lambda = 425$ nm, rather than a well-defined peak. Increasing ε_m also produces a red shift of the silver dipole LSPR respect to the higher order modes (which are at almost the same wavelengths in vacuum). This feature is revealed by the broadening and decreasing intensity of $Q_{abs,Ag}$. In this spectral range the enhancement of $Q_{sca,Ag}$ and $Q_{sca,Au}$ at 400 and 415 nm, respectively, are also important. On the spectral range between 500 and 600 nm, $Q_{abs,Au}$ has the main contribution to the extinction maximum at $\lambda = 534$ nm. However, the increments of $Q_{sca,Au}$ and $Q_{sca,Ag}$ at λ around 545 nm produced by changing the dielectric environment are very significant. Moreover, $Q_{abs,Ag}$ also shows a moderate but appreciable increment at 540 nm. This analysis indicates that, for this heteronanostructure, changing ε_m modifies the relationship between Q_{sca} and Q_{abs} in a complex manner.

We will now analyze the peak values of Q_{ext}, i.e., the $\lambda_{res,Ag}$ and $\lambda_{res,Au}$ data as a function of ε_m for $D = 50$ nm at several σ values. The results depicted in Figure 8 show that at a fixed diameter of the NP pair, the spectral position of the extinction peak associated to the Ag nanosphere redshifts almost linearly as ε_m increases, whatever the separation between the spheres (blue points). Moreover, the enhancement of the sensitivity of $\lambda_{res,Ag}$ with ε_m as the interparticle distance decreases is very remarkable. The dependence of $\lambda_{res,Au}$ on ε_m follows qualitatively the same trend of that of $\lambda_{res,Ag}$; however, for this extinction peak, the magnitude of the redshift is smaller at the same σ values. Note that this behavior is the result of all of the contributions described above. The same qualitative behavior was found for all the heterodimer of different sizes studied here, being the slope of the dependence of λ_{res} on ε_m proportional to D. This fact means that the sensitivity of the spectral position of the respective extinction peaks to a change in ε_m, at constant σ, is greater as D is increased, a relevant issue to be considered, for instance, in the design and development of plasmonic (bio)sensors.

Conclusions

In this work we have performed a systematic study of the far field optical properties of heterodimers composed of Ag and Au nanospheres both of the same diameter, in the range between 10 and 50 nm, using exact GMM electrodynamics calculations. In particular, we have analyzed the effect of the incident polarization, nanosphere separation, radius, and dielectric media on the optical response, as well as we have characterized the angular distribution of the scattered radiation on resonance with the extinction peaks of the heterodimers. The most attractive optical features are found for incident polarization parallel to the heterodimer axis. In this case, the extinction spectrum is characterized by two peaks associated to the dipole LSPR of the Ag and Au nanosphere, respectively. In turn, these two extinction peaks are significantly red-shifted as the interparticle distance is decreased, as their size is increased and as the dielectric constant of the environment is increased. The presence of these two plasmonic shifts in the extinction spectra, instead of only one as observed for homodimers, constitutes a novel characteristic feature which makes them different with respect to the widely studied homodimers. We propose that by knowing the respective λ_{res} values it could be possible to determine simultaneous and unambiguously both the size and interparticle

separation of a given heterodimer by means of two calibration curves. The on resonance scattered radiation of the heterodimer indicates that both plasmonic modes have a dipole character. As a consequence of the broken symmetry of the system we were able to analyze the contributions to extinction from each individual nanosphere, and verified the presence of Fano profiles coming from the relative contribution of absorption of the Au nanosphere, as it has been previously reported. Another novel and interesting finding in the present work is the observation, for the heterodimers with larger D, of quite unexpected increments in Q_{sca} in the off resonance particle, which could be interpreted as a process induced by near field coupling with the on resonance particle. Further studies on this near field energy transfer mechanism are in progress. We believe that the results presented in this work could be a useful guide for future experimental and theoretical studies of broken symmetry plasmonic systems.

Acknowledgment. Financial support from CONICET, FONCyT, ANTORCHAS, SECyT-UNC, and MinCyT-Córdoba is greatly acknowledged. E.R.E. thanks CONICET for a doctoral fellowship.

References and Notes

(1) El-Sayed, M. A. *Acc. Chem. Res.* **2001**, *34*, 257.
(2) Bohren, C. F.; Huffman, D. R. *Absorption and Scattering of Light by Small Particles*; Wiley-Interscience: New York, 1983.
(3) Kelly, K. L.; Coronado, E. A.; Zhao, L. L.; Schatz, G. C. *J. Phys. Chem. B* **2003**, *107*, 668.
(4) Le, F.; Brandl, D. W.; Urzhumov, Y. A.; Wang, H.; Kundu, J.; Halas, N. J.; Aizpurua, J.; Nordlander, P. *ACS Nano* **2008**, *2*, 707.
(5) Jiang, J.; Bosnick, K.; Maillard, M.; Brus, L. *J. Phys. Chem. B* **2003**, *107*, 9964.
(6) Nikoobakht, B.; El-Sayed, M. A. *J. Phys. Chem. A* **2003**, *107*, 3372.
(7) Willets, K. A.; Van Duyne, R. P. *Annu. Rev. Phys. Chem.* **2007**, *58*, 267.
(8) Crooks, R. M.; Zhao, M.; Sun, L.; Chechik, V.; Yeing, L. K. *Acc. Chem. Res.* **2001**, *34*, 181.
(9) Narayanan, R.; El-Sayed, M. A. *J. Phys. Chem. B* **2005**, *109*, 12663.
(10) Kamat, P V.; Schatz, G. C. *J. Phys. Chem. C* **2009**, *113*, 15473.
(11) Kamat, P. V. *J. Phys. Chem. C* **2008**, *112*, 18737.
(12) Kamat, P. V. *J. Phys. Chem. C* **2007**, *111*, 2834.
(13) Tabor, C.; Murali, R.; Mahmoud, M.; El-Sayed, M. A. *J. Phys. Chem. A* **2009**, *113*, 1946.
(14) Jain, P. K.; Huang, W.; El-Sayed, M. A. *Nano Lett.* **2008**, *8*, 43470.
(15) Sonnichsen, C.; Reinhard, B. M.; Liphardt, J.; Alivisatos, A. P. *Nat. Biotechnol.* **2005**, *23*, 741.
(16) (a) Reinhard, B. M.; Siu, M.; Agarwai, H.; Alivisatos, A. P.; Limphardt, J. *Nano Lett.* **2005**, *5*, 2246. (b) Reinhard, B. M.; Sheikholeslami, S.; Mastroianni, A.; Alivisatos, A. P.; Limphardt, J. *Proc. Natl. Acad. Sci. U.S.A.* **2007**, *104*, 2667. (c) Rong, G.; Wang, H.; Skewis, L.; Reinhard, B. M. *Nano Lett.* **2008**, *8*, 3386.
(17) Jain, P. K.; Huang, W.; El-Sayed, M. A. *Nano Lett.* **2007**, *7*, 2080.
(18) Tamaru, H.; Kuwata, H.; Miyazaki, H.; Miyano, K. *Appl. Phys. Lett.* **2002**, *80*, 1826.
(19) Hao, E.; Schatz, G. C. *J. Chem. Phys.* **2004**, *120*, 357.
(20) Gunnarson, L.; Rindzevicius, T.; Prikulis, J.; Kasemo, B.; Kal, M.; Zou, S.; Schatz, G. C. *J. Phys. Chem. B* **2005**, *109*, 1079.
(21) Su, K. H.; Wie, Q. H.; Zhang, X.; Mock, J. J.; Smith, D. R.; Schultz, S. *Nano Lett.* **2003**, *3*, 1087.
(22) Rechberger, W.; Hohenau, A.; Leitner, A.; Krenn, J. R.; Lamprecht, B.; Aussenegg, F. R. *Opt. Commun.* **2004**, *4*, 899.
(23) Wang, H.; Reinhard, B. M. *J. Phys. Chem. C* **2009**, *113*, 11215.
(24) Claro, F. *Phys. Rev. B* **1984**, *30*, 4948.
(25) Rojas, R.; Claro, F. *Phys. Rev. B* **1986**, *34*, 3730.
(26) Olivares, I.; Rojas, R.; Claro, F. *Phys. Rev. B* **1987**, *35*, 2453.
(27) Purcell, E. M.; Pennypacker, C. R. *Astrophys. J.* **1973**, *186*, 705.
(28) Gérardy, J. M.; Ausloos, M. *Phys. Rev. B* **1982**, *25*, 4204.
(29) Chergui, M.; Melikian, A.; Minassian, H. *Phys. Chem. C* **2009**, *113*, 6463.
(30) Nordlander, P.; Oubre, C.; Prodan, E.; Li, K.; Stockman, M. I. *Nano Lett.* **2004**, *4*, 899.
(31) Prodan, E.; Nordlander, P. *J. Chem. Phys.* **2004**, *120*, 5444.
(32) Yang, L.; Wang, H.; Yan, B.; Reinhard, B. M. *J. Phys. Chem. C* **2010**, *114*, 4901.
(33) Encina, E. R.; Coronado, E. A. *J. Phys. Chem. C* **2010**, *114*, 3918.
(34) Pinchuk, A. O.; Kalsin, A. M.; Kowalczyk, B.; Schatz, G. C.; Grzybowski, B. A. *J. Phys. Chem. C* **2007**, *111*, 11816.
(35) Bachelier, G.; Russier-Antoine, I.; Benichou, E.; Jonin, C.; Del Fatti, D.; Vallée, F.; Brevet, P. F. *Phys. Rev. Lett.* **2008**, *101*, 197401.
(36) Xu, Y. *Appl. Opt.* **1997**, *36*, 9496.
(37) Xu, Y.; Wang, R. T. *Phys. Rev. E* **1998**, *58*, 3931.
(38) *Handbook of Optical Constant of Solids*; Palik, E. D., Ed.; Academic Press: New York, 1985.
(39) García de Abajo, F. J. *J. Phys. Chem. C* **2008**, *112*, 17983.
(40) Sheikholeslami, S.; Jun, Y.; Jain, P.; Alivisatos, A. *Nano Lett.* **2010**, *10*, 2655.
(41) Muskens, O. L.; Bachelier, G.; Del Fatti, N.; Valle'e, F.; Brioude, A.; Jiang, X.; Pileni, M. *J. Phys. Chem. C* **2008**, *112*, 8917.
(42) Muskens, O. L.; Billaud, P.; Broyer, M.; Del Fatti, N.; Valle'e, F. *Phys. Rev. B* **2008**, *78*, 205410.
(43) Muskens, O. L.; Christofolos, D.; Del Fatti, N.; Valle'e, F. *J. Opt. A: Pure Appl. Opt.* **2006**, *8*, 264.

JP105522B